



Fermi National Accelerator Laboratory

FERMILAB-TM-1743

Some Design Considerations for Pbar Target Sweeping Station

C. M. Bhat

Fermi National Accelerator Laboratory

P.O. Box 500

Batavia, Illinois 60510

June 1991



Operated by Universities Research Association Inc. under contract with the United States Department of Energy

Some Design Considerations for Pbar Target Sweeping Station

C.M. Bhat

Fermi National Accelerator Laboratory
P.O. Box 500, Batavia, Illinois 60510

1 Introduction

This report summarizes the results of some recent calculations useful to design the beam sweeping station to produce high intensity pbar beam at AP0 and is a follow-up of our previous reports(Ref. 1). With various on-going and planned intensity upgrade at the accelerator including the main injector (Ref. 2) the primary beam intensity on the pbar target is expected to increase from about 2.0×10^{12} to 5.0×10^{12} protons/pulse (or higher) at a repetition rate of one pulse/1.5sec. The beam spot size σ ($= \sigma_x = \sigma_y$) on the target could go as small as 0.01 cm or smaller. The intensity increase and/or beam spot size decrease on the target is done in order to increase phase space density of the pbars collected at the debuncher. But some complications would arise from the existing method of pbar production i.e. by bombarding the proton beam directly on a chunk of metal. A study of the heavy metal targets used in the 1987 collider run (Ref. 3) when the beam intensity was about 1.0×10^{12} , has shown a clear indication of target destruction by the proton beam. It has been inferred that the source of the target damage is due to the large local variations of the material density induced by the beam. Although the heavy metal has very high melting point temperature the thermoelastic property is not suitable for its use as a reliable pbar target. During 1989 collider run, the target material was changed over to copper because of its better thermoelastic properties. A beam intensity of 2.2×10^{12} protons per pulse was reached and the pbar yield measurement did not show much indications of target destruction except for a small (nearly 6 to 7 %) decrease in the pbar yield. However, the calculations showed that the target material along the beam might have had enough energy deposition to transform the target material

from the solid state to the liquid state (at NTP) during the beam spill time. A further increase of the proton beam intensity might cause melting of the target and drill a hole. Hence it is suspected that a major decrease in the energy deposited per unit volume may be required.

These problems stimulated an investigation of suitable target materials and a method to handle the high intensity proton beam. Properties of a number of target materials have been studied in terms of their mechanical strength/resistance to shock-waves i.e. their thermoelastic behaviour. The relative pbar yields have also been considered. To handle the beam on the target, the beam sweeping technique (Ref. 1,4) seems to be one of the promising methods. In this scheme, the high intensity proton beam will be swept circularly with a sweeping radius of $> 0.33\text{mm}$ at a frequency of $.6\text{MHz}$, so that at any point on the target the maximum density of energy deposition will not exceed the melting point energy of the target material. The beam sweeping can be achieved by two pairs of kickers excited by a sinusoidal wave: one pair at the up-stream of the target and one pair at the down-stream of the target. The energy deposition in the up-stream pair of kickers is much smaller compared to the down stream kicker magnets. Hence, the design considerations of the former magnets are rather straight forward. On the other hand the requirements and the limitations for the down stream magnets should be examined carefully. An accurate estimate of energy deposition/temperature distributions and star density caused by the secondaries become the key points in deciding the short and long term behaviour of these kickers as well as other devices in the beam line.

2 Selection of Target Material

The primary beam of $1.6\mu\text{sec}$ pulse width dumps the energy into the target and the downstream devices almost instantaneously. This sudden change in energy density dE and the corresponding change in hydrostatic pressure dP in the material are related by Mie-Gruneisen equation of state (Ref. 5) given by

$$dP = \gamma\rho dE \quad (1)$$

where γ is the Gruneisen parameter

$$\gamma = \frac{B_T(3\alpha)}{\rho C_V}$$

B_T , α and C_V are bulk modulus, coefficient of expansion at $20^\circ C$ and mean specific heat respectively. ρ is the density of the material. This parameter is useful in determining the response of the material to rapid heating at

Table 1. Thermoelastic properties of some target materials.

Material	Density (gm/cc)	Thermal Conductivity (W/m-K°)	$\gamma \rho$ (gm/cc)	Melting Point Energy J/gm
Al	2.7	238	5.99	1064
Ti	4.5	21.6	5.57	1357
Co	8.9	100	15.90	1232
Cu	8.96	394	17.87	668
Ag	10.5	419	25.30	326
W [¶]	19.3	167	30.42	751
Ir	22.4	148	57.95	537
Au	19.3	293	55.64	352

¶ Heavy metal is an alloy of 90 % of W 6 % of Cu and 4 % of Ni. Therefore properties of heavy metal is assumed to be mainly from W.

constant volume. γ does not change significantly with energy change dE. Pressure developed at any point in the material due to a single beam pulse is believed to be the main source of the mechanical distortion produced by the beam and the sudden pressure variation along the beam path within the beam spill time is the triggering point of shock waves in the medium. If the pressure in the decompressive region can fall below certain critical value decided by the elastic limit, a permanent destruction of the material could take place. Table 1 gives the properties of some target materials. The extracted values of $\gamma \rho$ and the melting point energies are given in the last column. The linear relationship between dP and dE shown in figure 1, clearly indicates

that for the same amount of energy deposition heavy metal experiences about twice the pressure as compared to copper while iridium experiences about four times the pressure. Some of the target materials given in table 1 have favourable melting point energies but their densities are small. The target material has to be a good conductor of heat so that quick heat dissipation takes place. Therefore we conclude that copper is a suitable target material. We have not studied the feasibility of using other alloys, however.

3 Calculations of Energy Deposition

Energy deposition per proton pulse has been calculated using inclusive simulation of three dimensional hadron and electromagnetic cascades in the target and beam-line devices down-stream. We have used the Monte Carlo code MARS10 (Ref. 6) and the results have been compared to results obtained (not presented here) from CASIM (Ref. 7). A block diagram of the devices used in the calculations is shown in figure 2. We assume cylindrical geometry throughout. The dimensions of these devices have been taken from Ref. 8. Slight changes in the final design of the sweeping station will not change our predictions.

To evaluate maximum energy density deposited in a material the grid size to be used in the calculations plays a very important role. A systematic study has shown that to make a realistic estimation of maximum energy density along the beam (e.g. in case of a target or a beam dump) one might choose an optimum radial grid size, ΔR , of the order of 0.5σ for the first few radial sub-sections in the material, while for regions away from the beam axis one may choose larger steps. Ref. 1 presents the results of calculations for target with optimum step-sizes selected based on this criteria for sweeping radius of .025cm. In the case of the kickers we use a minimum grid size of 4σ for the first four interior radial zones to estimate maximum energy density and we increase the radial grid size to a maximum value of 1.91cm for the subsections near the edges of the magnet. Throughout these calculations we assume a sweeping radius of .05cm. and a $\sigma = .01$ cm.

For the down stream kickers the ferrite MN67 is suggested to be a suitable material (Ref. 8) because of its high electrical resistivity and magnetic permeability. Calculations have been carried out for two different types of magnetic materials viz., iron and ferrite. Some of the important properties

of these materials are given in the table 2.

Figure 3 presents average energy density distribution for the target and the Li-lens. Integrated energy deposition in the target as a function of radial distances for four different target lengths $L = 5, 7, 9$ and 11 cm are shown in the figure 4. These Monte-Carlo data can be explained by a simple relation

$$\begin{aligned} E_{Tot} &\approx f(L)g(R) \\ &= \eta 10^{\eta L} (1.0 + \xi \text{Log} R) \end{aligned} \quad (2)$$

where $\eta = 0.135$, $\xi = 0.3$ and L is depth of the target along the beam. Figure 5 shows our predictions for the radial distribution of energy density for iron and ferrite core magnets, with the Li lens on and off. Figure 6 gives a comparison of radial distribution of average energy density in the two sweeping magnets with the Li lens on. We generally operate the Li lens at about 0.5MAmp pulse in the secondary. The difference between the total energy deposition with lens off and on is small. Therefore no attempts have been made to look for the systematics of energy deposition in the down stream devices as a function of current intensity in the lens (i.e. with different magnetic fields in the lens). Table 3 illustrates total amount of energy deposited in various devices in the beam line as a result of one beam particle interaction in the target. The differential energy density distributions in the entire sweeping station is shown in figure 7.

One of the important consequences of change in energy density (or pressure) in the material is the subsequent instantaneous increase in the temperature. An exact evaluation of the temperature rise along the beam in the target is difficult. However, we can make an approximate estimation by solving the equation,

$$dE = aT + \frac{1}{2}(b \times 10^{-3})T^2 + \frac{1}{3}(c \times 10^{-6})T^3 - \frac{d \times 10^5}{T} - A \quad (3)$$

a, b, c, d and A are constants (Ref. 9) obtained by fitting the experimental data. T is the absolute temperature in $^{\circ}K$. dE is the change in energy density. This equation assumes energy change at constant pressure. Hence we may under estimate the temperature rise. The steady state temperature of a device is decided by the average thermal conductivity of the material and the rate at which the device is being cooled down by an external cooling system.

The temperature change/increase could be a serious problem especially to magnetic devices like kickers, pulsed magnets etc., built using ferro-magnetic materials because above the transition temperature they cease to be

Table 2. Magnetic materials to build down stream kickers in the target sweeping station and their properties.

Material Name	Density (gm/cc)	Resistivity Ohm-m	Transition Temp. (C°)	Thermal Conductivity (W/m-K°)
Fe	7.87	0.101E-6	770	80.4
Ferrite	4.8	4.0	> 200	4-7E-6
MN67¶				

¶ Ferrite MN67 has an equivalent chemical formula as $Fe_{2.27}O_4Mn_{.458}Zn_{.274}$ and is assumed to have $Z_{eff} = 15.8$ and $A_{eff} = 33.42$ for the calculations.

Table 3. Total energy deposited in the down stream devices

Device Name	Total Energy Deposited (GeV/proton)¶	
	Li-Lens off	Li-Lens on
Target	1.90	1.89
Li lens	0.11	0.10
Lens Transf.	6.68	6.86
Kicker 1	2.54	2.59
Kicker 2	2.43	2.25
Pulsed Magnet		7.1¶¶

¶ To obtain energy in joule multiply total energy by $1.602N_p \times 10^{-10}$.

¶¶ This result is obtained by a calculations with CASIM. The energy deposition could be about 30 % smaller than the MARS10 predictions.

magnetic. Figure 8 presents a comparison for instantaneous temperature rise in the kicker arising from a primary beam of intensity 5×10^{12} protons/pulse. We find a maximum temperature gradient of 1.8° K/cm for ferrite and 9.2° K/cm for iron magnets.

The total energy deposition, star density and temperature rise per pulse in these devices are linear functions of the beam intensity for a given proton beam energy. This implies that, at increased primary beam intensities all the down stream devices are going to receive larger amounts of radiations. The calculations shows that for primary intensity beam of $2E12$ protons/pulse the maximum energy deposited in the down stream lithium lens transformer is about 2230 Joule. In the Main injector era one expects that the primary beam intensity would be increased by about 2-3 times the present Main ring beam intensity. Hence the energy deposition in the lens transformer would also go up nearly by the same factor. This suggests that the present design of lens transformer may have to be improved to handle higher beam intensities. Also a careful design of the down stream magnets has to be made so that proper heat dissipation takes place within the pulse-repetition time and also the steady state temperature should not exceed the transition temperature.

Author would like to thank J. Marriner and M. Gormley for useful comments.

REFERENCES

1. C.M. Bhat and N.V.Mokhov, Fermilab, TM1585 (1989), C.M. Bhat, Pbar Note 485 (1989).
2. Fermilab Upgrade Phase II: The Main Injector, January (1990).
3. M.Gormley, Fermilab private communications (1988).
4. F.Krienen and F.Mills, Fermilab PBAR Note-70 (1980).
5. G.H.Bloom, AIP Proceedings 94, (1982) 588
6. N.V. Mokhov, MARS10 Manual, Fermilab, FN-509 (1989).
7. A. Van Ginneken, CASIM, Fermilab FN-272 (1975).
8. C. Crawford (private communication)(1989).
9. Hand Book of Physics and Chemistry 1989-90 page D-42.

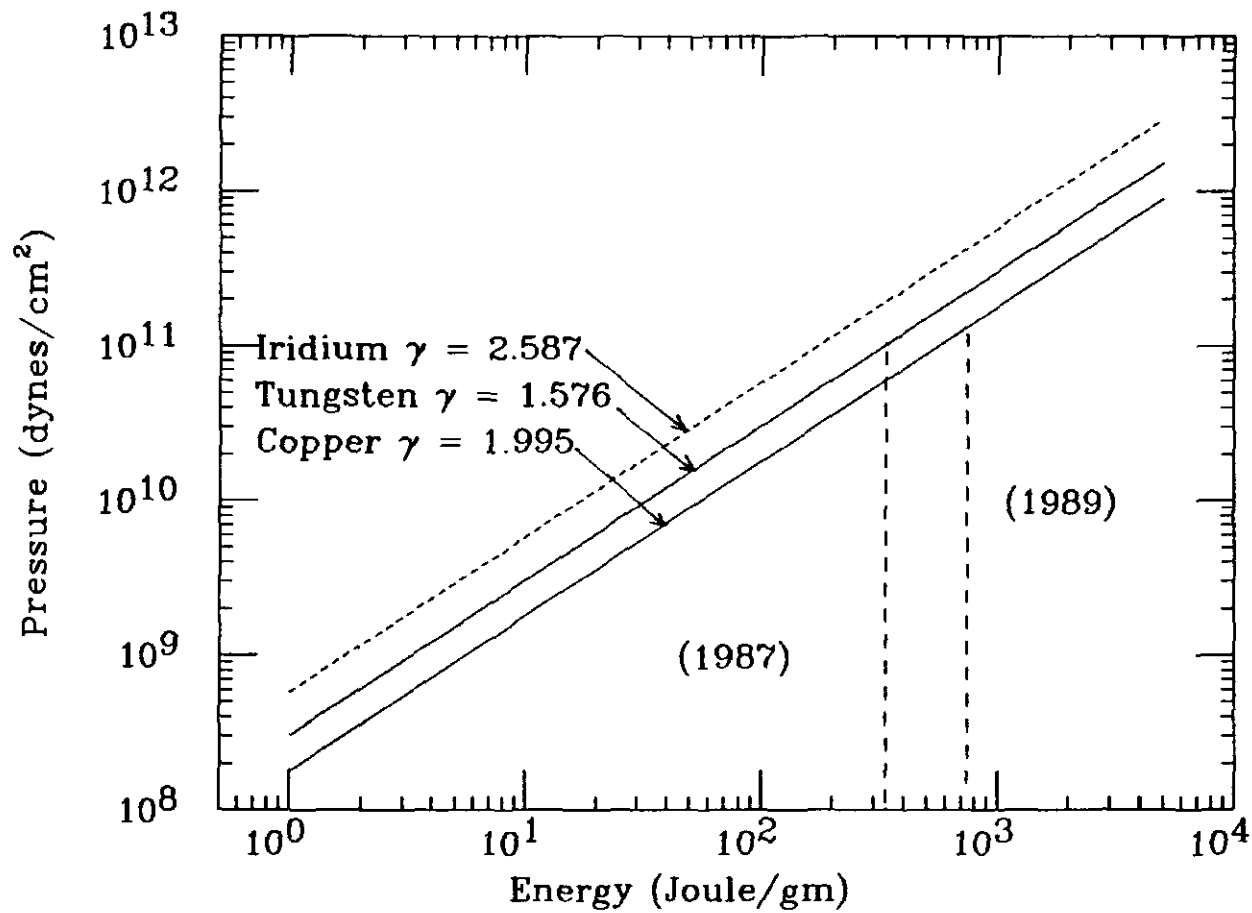


Fig. 1. Pressure versus sudden change in energy density in copper, iridium and tungsten. Vertical lines indicate the calculated maximum energy density deposited during 1987 (336J/gm p-p) and 1989 (740 J/gm p-p) collider runs.

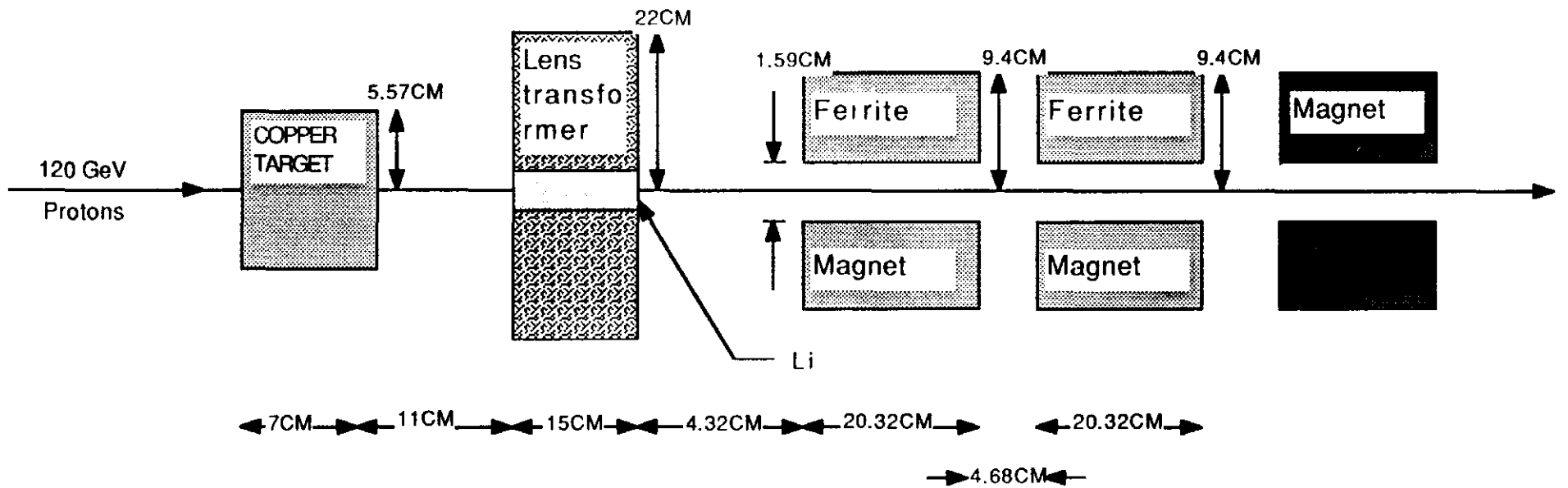


Fig. 2. Block diagram of beam sweeping station. The figure is not to the scale.

$$E_p = 120\text{GeV}/c, \sigma = .01\text{cm}, \text{ppp} = 5 \cdot 10^{12}$$

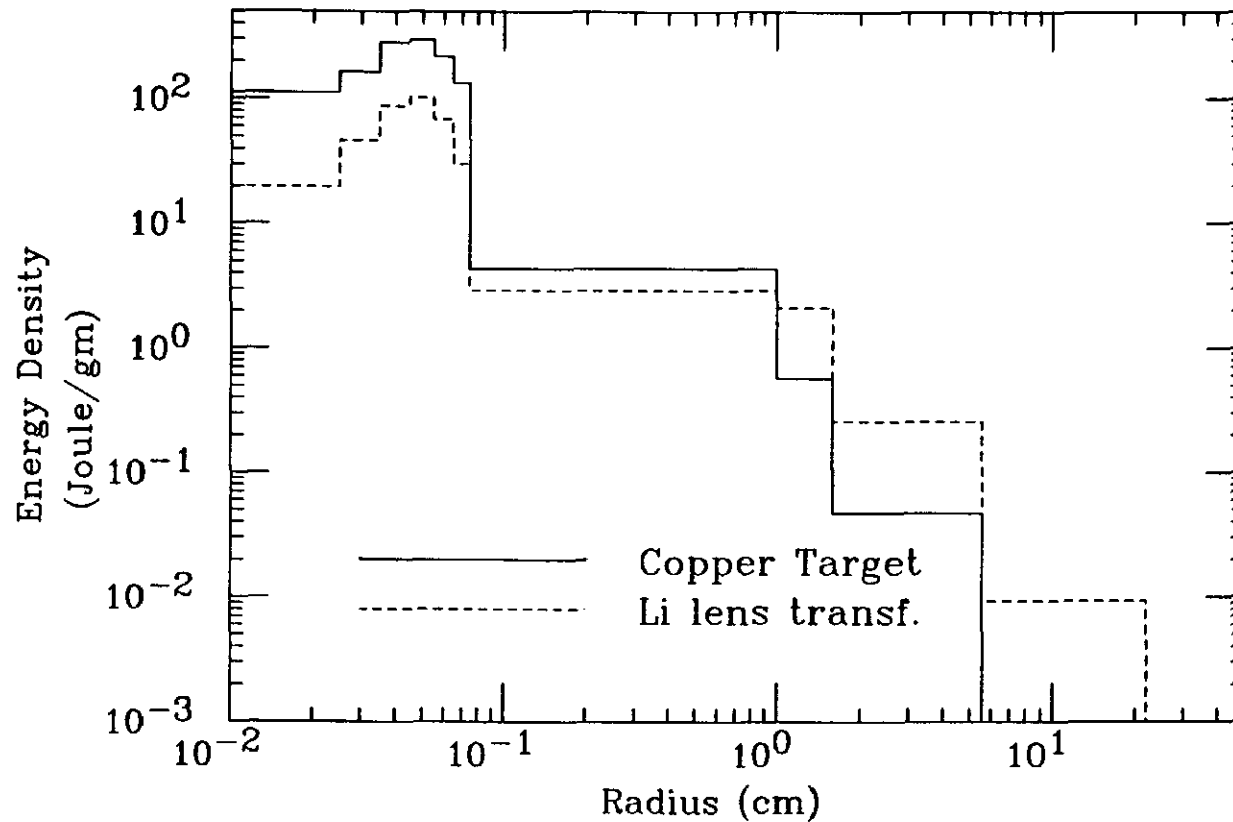


Fig. 3. Average energy density distribution in the target and Li lens with lens on. A cylindrical lithium lens of 1.0cm radius with iron transformer is assumed for the calculation.

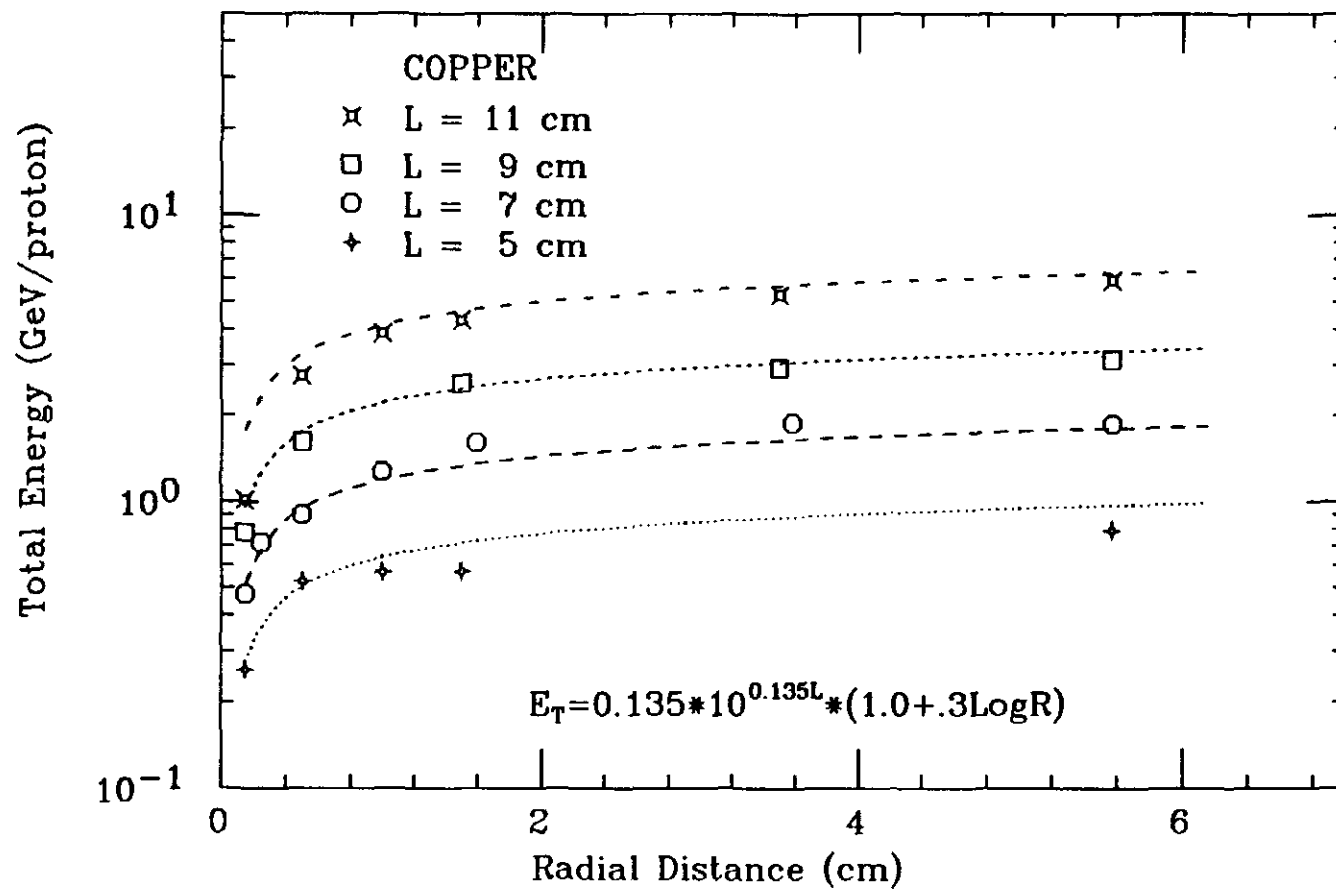


Fig. 4. Integrated energy deposition in the target versus the target thickness. The lines indicate a fit to the data obtained from Monte Carlo calculations.

$$E_p = 120\text{GeV}/c, \sigma = .01\text{cm}, \text{ppp} = 5 \cdot 10^{12}$$

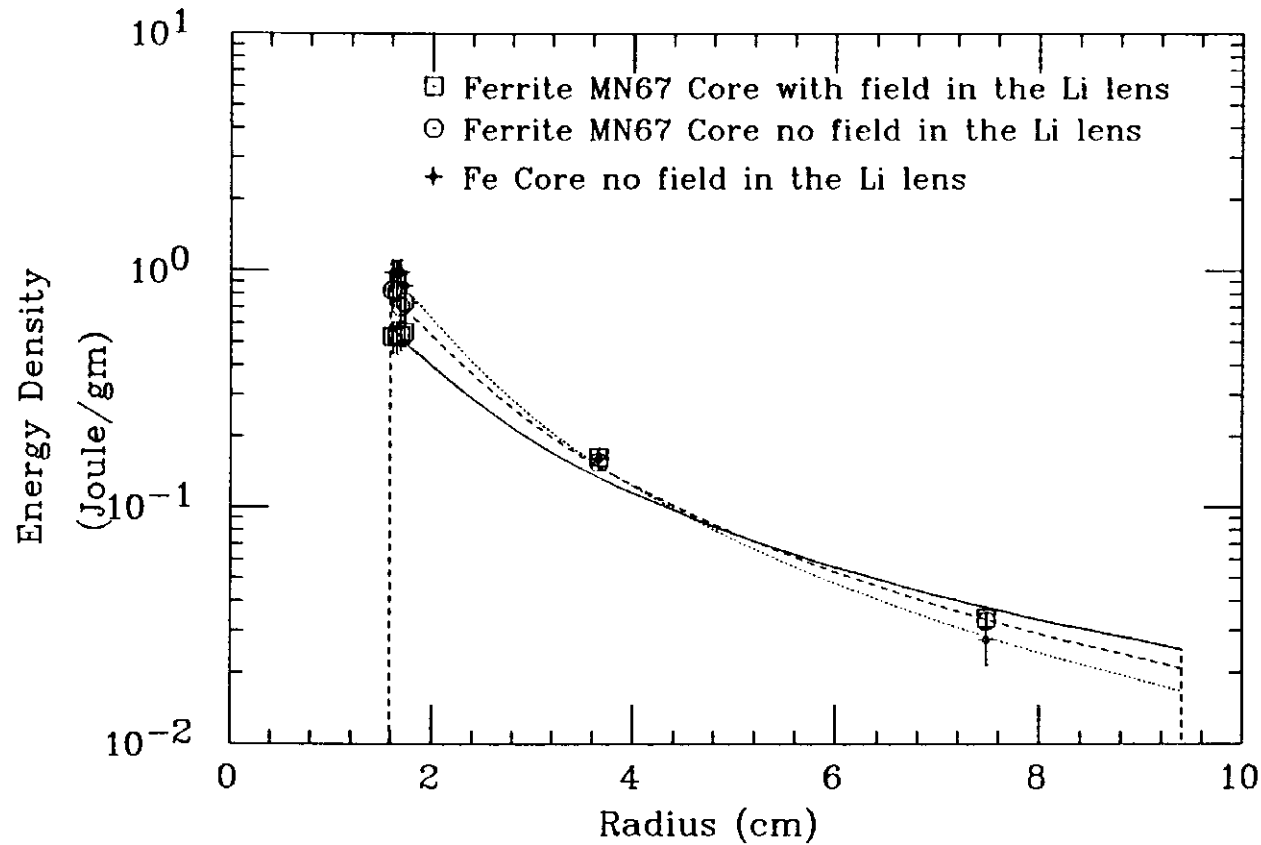


Fig. 5. A comparison of average energy density deposition in the first down stream kicker magnet with iron and ferrite MN67 core. The lines are results of logarithmic fit to the data predicted by MARS10. A beam sweeping radius of .05cm is assumed in these calculations.

$$E_p = 120\text{GeV}/c, \sigma = .01\text{cm}, \text{ppp} = 5 \times 10^{12}$$

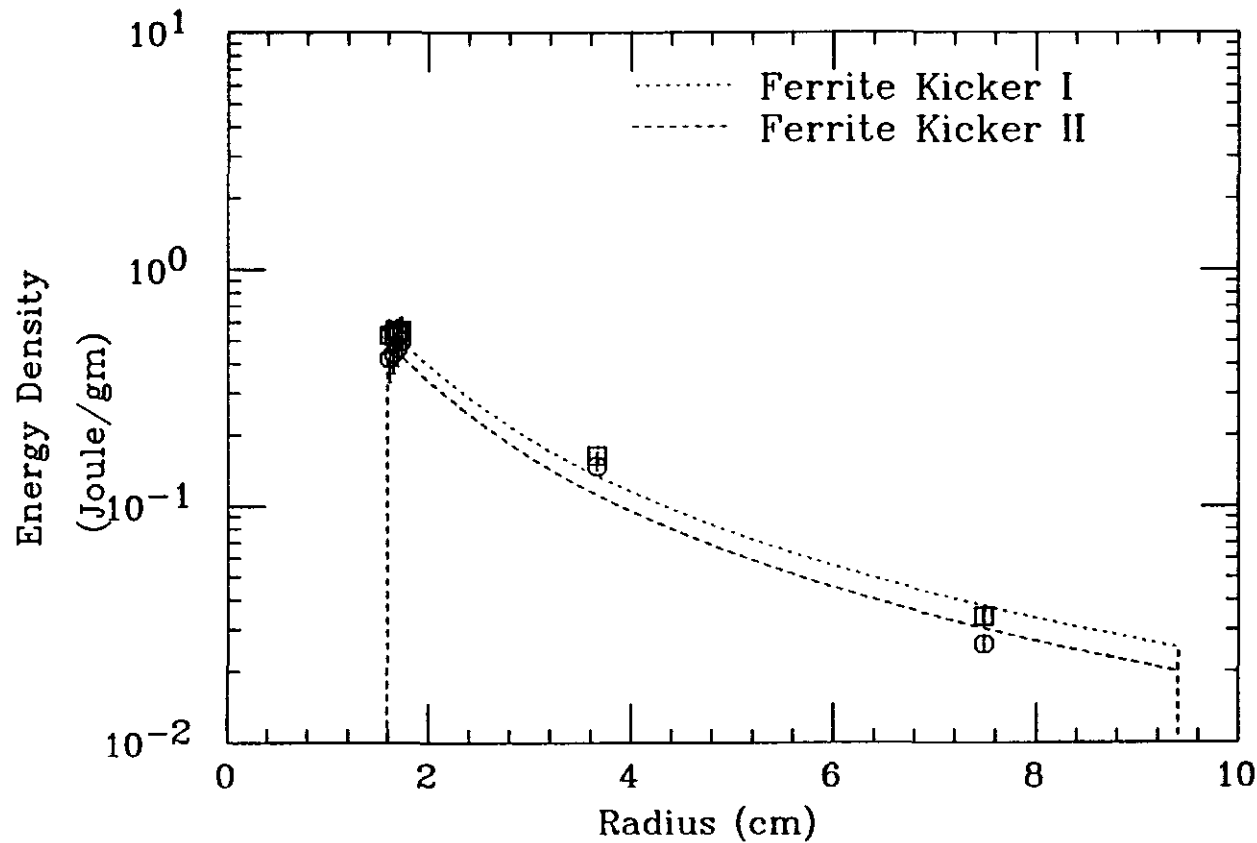


Fig. 6. A comparison of average energy density deposition in the down stream kickers magnet made up of ferrite MN67. The lines are results of logarithmic fit to the data predicted by MARS10. The calculations assumes a 0.5MAmp of current the secondary of the Li lens.

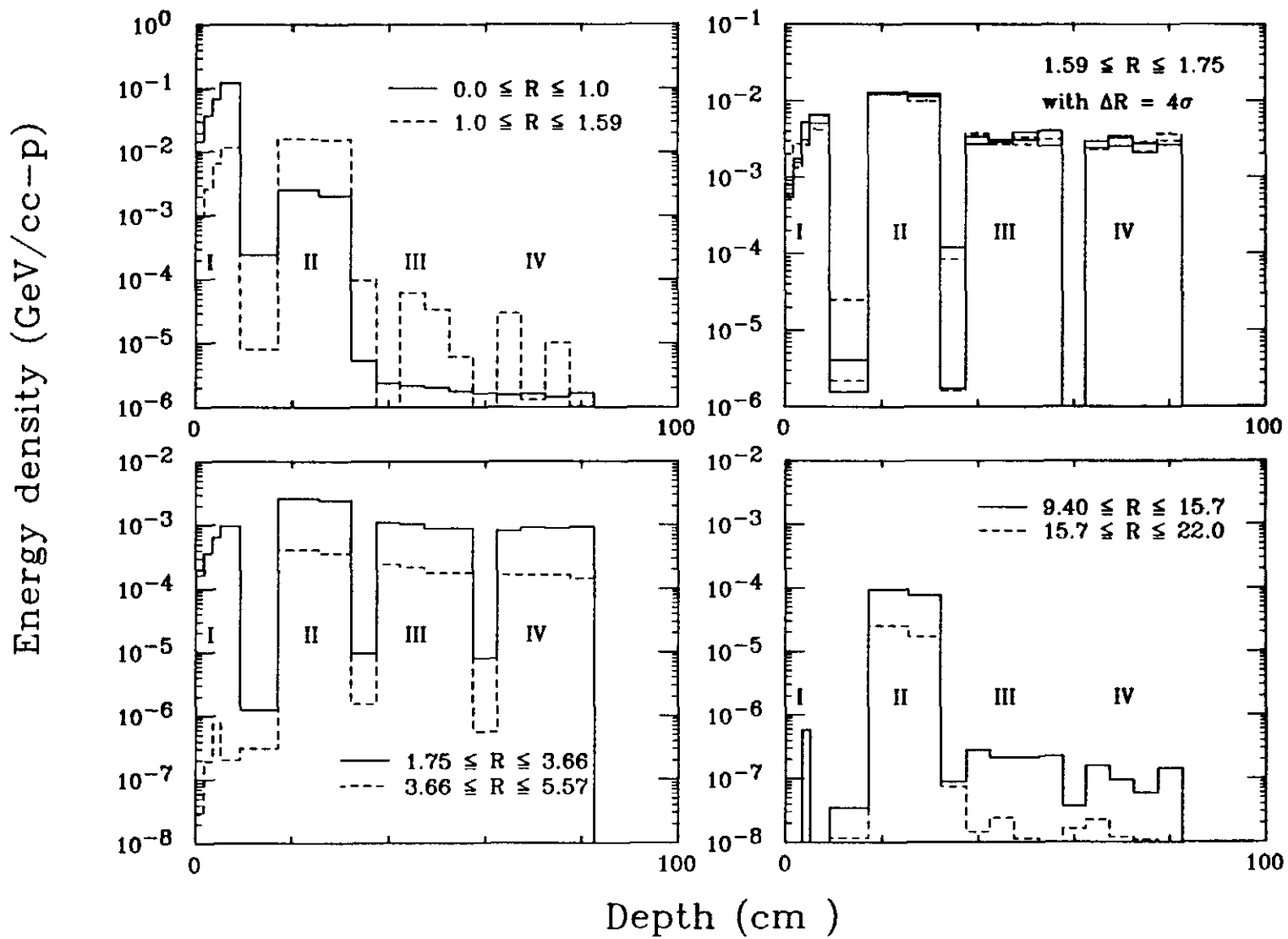


Fig. 7. A differential energy density distribution in the sweeping station devices resulting from an interaction of 120 GeV proton beam particle. Meaning of the regions are I : Cu target, II : Li lens with transformer, III : First ferrite magnet and IV : Second ferrite kicker magnet.

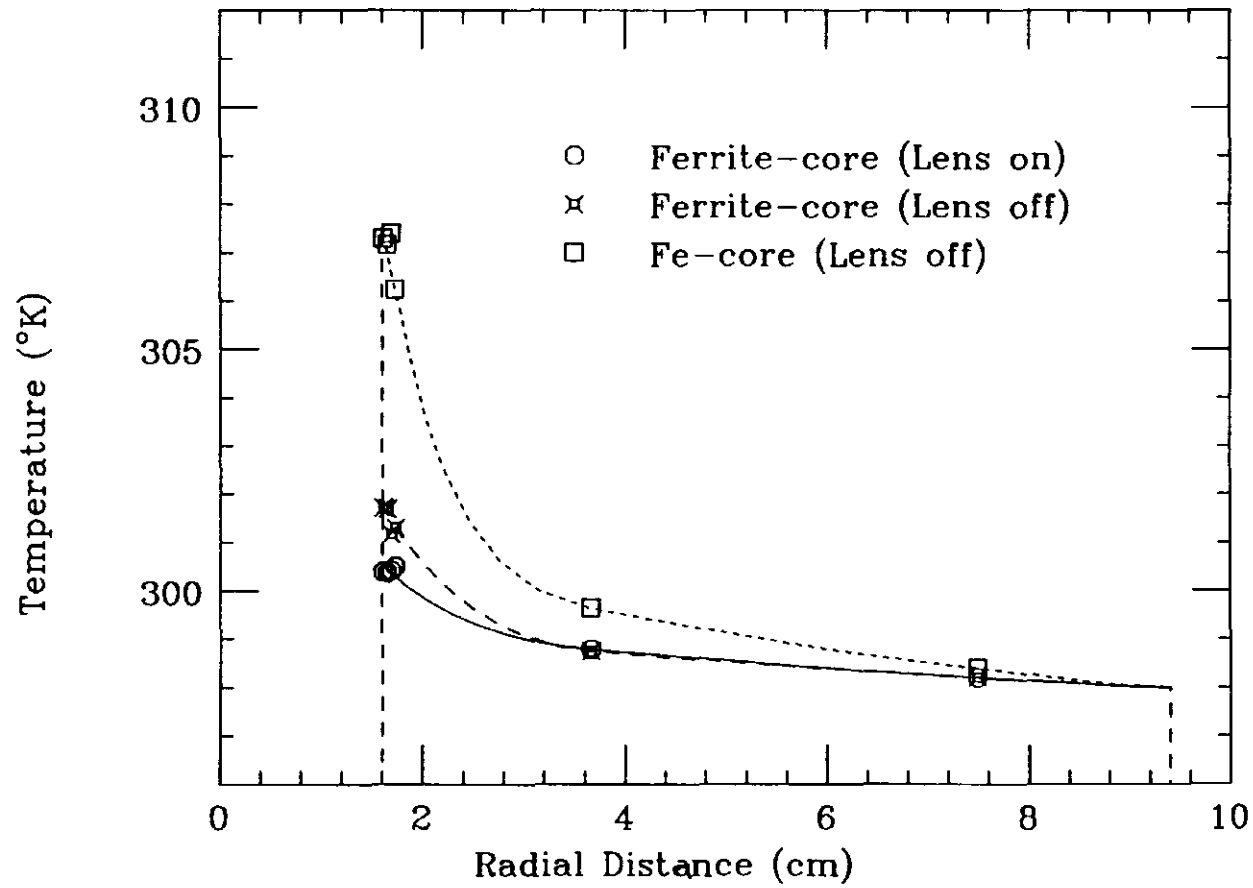


Fig. 8. An average instantaneous temperature rise in the first down stream kicker magnet as a result of the interaction of primary proton beam of intensity $5E+12$ protons/pulse.